# Situation-Aware Adaptive Transmit Beamforming for Automotive Radars

Focante, Edoardo; Myers, Nitin Jonathan; Joseph, Geethu; Pandharipande, Ashish

**DOI**
10.1109/ICASSP48485.2024.10447374

**Publication date**
2024

**Document Version**
Final published version

**Published in**
Proceedings of the IEEE International Conference on Acoustics, Speech and Signal Processing, ICASSP 2024

ICASSP 2024 - 2024 IEEE International Conference on Acoustics, Speech and Signal Processing (ICASSP) | 979-8-3503-4485-1/24/$31.00 ©2024 IEEE | DOI: 10.1109/ICASSP48485.2024.10447374

# SITUATION-AWARE ADAPTIVE TRANSMIT BEAMFORMING FOR AUTOMOTIVE RADARS

*Edoardo Focante*[1], *Nitin Jonathan Myers*[1], *Geethu Joseph*[2], *Ashish Pandharipande*[3]

[1]Delft Center for Systems and Control, Delft University of Technology, The Netherlands
[2]Signal Processing Systems, Delft University of Technology, The Netherlands
[3]NXP Semiconductors, The Netherlands

## ABSTRACT

Millimeter-wave radar is a common sensor modality used in automotive driving for target detection and perception. These radars can benefit from side information on the environment being sensed, such as lane topologies or data from other sensors. Existing radars do not leverage this information to adapt waveforms or perform prior-aware inference. In this paper, we model the side information as an occupancy map and design transmit beamformers that are customized to the map. Our method maximizes the probability of detection in regions with a higher uncertainty on the presence of a target. Simulation results on the nuScenes dataset show that the designed beamformer achieves substantially higher detection rates than a conventional omnidirectional beamformer for the same transmitted power.

***Index Terms*—** Automotive radar, situation-aware transmit beamforming, occupancy grid, cognitive radar.

## 1. INTRODUCTION

Millimeter-wave radars are currently employed in automobiles to achieve enhanced perception, even in challenging weather conditions [1–4]. These radars often operate alongside other sensors, such as cameras, GPS, and LiDARs, that provide useful information on the environment being sensed. For example, location information from GPS can be used together with lane topology maps to determine static obstructions in the environment, such as lamp posts, buildings, and guardrails. An automotive radar can make use of such side information to dynamically adjust the waveforms at the transmitter and adapt detection algorithms at the receiver. By leveraging the side information available at the vehicle, radars can significantly enhance their sensing capabilities.

A common approach to model the information from different sensors is to use an occupancy grid map [5–7], which is a function defined over a grid of cells in the environment. Each cell can represent a range-angle-Doppler bin of interest, and the occupancy map value at a cell is the probability that the cell is occupied by an object. An occupancy map is typically generated by processing point cloud data obtained from various sensors, using predictive models that track objects, or by a combination of both. With the knowledge of an occupancy map, a good sensing strategy is one that emphasizes target detection at cells associated with higher uncertainty. A radar can realize such a sensing strategy by adapting its transmitted waveforms and its algorithms to the map.

Prior work has studied the use of side information in both waveform design and algorithm design for radars. For instance, clutter covariance information was used in [8] and [9] to maximize target detection performance under clutter. Specifically, space-time beamformers were designed in [8], and the transmit waveform and the receive filter were optimized in [9]. This paper assumes that the clutter is non-dominant and it can be treated as noise. In [10] and [11], receive algorithms were developed to exploit the angle-of-arrival statistics for localization. The transmit processing in [10] and [11], however, was agnostic to the angle-domain statistics. In [12], an airborne radar was used to search and track a swarm of targets. In particular, a beam with a fixed pattern and fixed beamwidth was continuously steered in azimuth and elevation to the region of maximum uncertainty. Several metrics, including entropy, are discussed in [12] to quantify uncertainty in a region. The approach in [12], however, does not fully harness the potential of typical antenna arrays, which have the ability to dynamically adjust the beam's size and pattern. Furthermore, as the beams in [12] only cover a fixed angular region, the method in [12] requires multiple beam scans even for static environments. Such a beam scanning approach might result in a substantial scanning overhead in typical automotive driving scenarios.

This paper proposes a method to dynamically adapt the transmit beamformer to a probabilistic occupancy map, assuming a standard detector at the receiver. The beamformer is obtained by maximizing a weighted sum of detection probabilities, where the weights are the entropies derived from the probabilistic map. Our designed beamformer focuses higher power in cells where the occupancy uncertainty is higher, thus enhancing detection in regions with higher uncertainty. Finally, we demonstrate, using the nuScenes dataset, the superior detection performance of our method over the omnidirectional operation that does not leverage occupancy maps.

## 2. SYSTEM MODEL

We consider an automotive radar with a co-located transmitter (TX) and receiver (RX). We assume half-wavelength spaced uniform linear arrays at the TX and the RX. Furthermore, we consider an analog beamforming architecture with $N_{\text{tx}}$ isotropic antennas at the TX and a digital array with $N_{\text{rx}}$ isotropic antennas at the RX, as shown in Fig. 1.

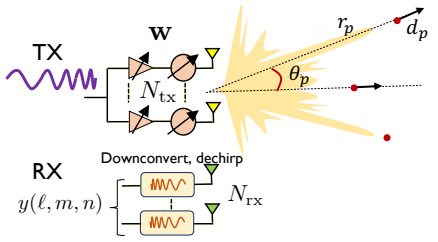


**Fig. 1:** The TX applies a beamformer $\mathbf{w}$ to its $N_{\text{tx}}$-element analog array. Our design adapts $\mathbf{w}$ to the occupancy map.

We assume that the TX periodically transmits linear frequency modulated continuous wave over a unit-norm analog beamformer $\mathbf{w} \in \mathbb{C}^{N_{\text{tx}}}$, i.e., $\|\mathbf{w}\|_2 = 1$. The beamformer $\mathbf{w}$ is fixed within a coherent processing interval, during which the occupancy grid map is assumed to be constant. We define $P_{\text{tx}}$ as the power transmitted by the TX. The transmitted signal impinges $P$ point targets within the radar's field of view. We define $\theta_p$ as the direction of departure associated with the $p^{\text{th}}$ target. The array response vector at the TX for direction $\theta$ is defined as

$$\mathbf{a}_{N_{\text{tx}}}(\theta) = [1, e^{-\text{j}\pi\sin\theta}, e^{-2\text{j}\pi\sin\theta}, \cdots, e^{-\text{j}\pi(N_{\text{tx}}-1)\sin\theta}]^T. \tag{1}$$

The TX can control the beamforming gain along direction $\theta$, i.e., $|\mathbf{w}^T\mathbf{a}_{N_{\text{tx}}}(\theta)|^2$, by designing the beamformer $\mathbf{w}$.

At the radar receiver, the reflected echoes are downconverted, dechirped, and sampled. The $\ell^{\text{th}}$ sample of the signal observed at the $n^{\text{th}}$ receive antenna in the $m^{\text{th}}$ slow-time slot is given by

$$y[\ell,m,n] = \sqrt{P_{\text{tx}}}\sum_{p=1}^{P}\left(\frac{\alpha_p \mathbf{a}_{N_{\text{tx}}}(\theta_p)^T\mathbf{w}}{r_p^2} \times e^{\text{j}(2\pi\ell\mu_p + 2\pi m\gamma_p - \pi n\sin\theta_p)}\right) + v[\ell,m,n], \tag{2}$$

where $r_p$ is the range associated with the $p^{\text{th}}$ target. Further, $\alpha_p$ and $\gamma_p$ are proportional to the radar cross section (RCS) and the Doppler shift $d_p$, and $\mu_p$ is the discrete-time beat frequency which is proportional to $r_p$. Finally, $v[\ell,m,n]$ is additive white Gaussian noise in the observed sample. The received measurement in (2) encodes the range, angle, and Doppler information of all the $P$ targets.

The received measurements are arranged in a 3D data cube defined by (2), and then processed using a 3D-discrete Fourier transform (DFT) to detect targets. We consider a discrete grid of $N_{\text{R}}$ range bins, $N_{\text{rx}}$ angle bins, and $N_{\text{D}}$ Doppler bins for the 3D-DFT. We assume that the $P$ targets are positioned on this discrete grid, resulting in orthogonal received responses from the targets. Under this assumption, $\theta_p$s are such that $\pi\sin\theta_p$ is an integer multiple of $2\pi/N_{\text{rx}}$. The bins within the 3D-DFT cube are indexed as $(i,j,k)$, and its entries indicate the presence of a target in a range-angle-Doppler bin of interest. When the $(i,j,k)^{\text{th}}$ range-angle-Doppler bin contains a target indexed $p$, the corresponding entry within the 3D-DFT cube is

$$\tilde{y}(i,j,k) = \sqrt{P_{\text{tx}}}\frac{\alpha_p \mathbf{a}_{N_{\text{tx}}}(\theta_p)^T\mathbf{w}}{r_p^2} + \tilde{v}(i,j,k), \tag{3}$$

where $\tilde{v}(i,j,k)$ is Gaussian noise with zero mean and variance $\sigma^2$. When there is no target in the $(i,j,k)^{\text{th}}$ bin, the 3D-DFT entry $\tilde{y}(i,j,k)$ is just the noise $\tilde{v}(i,j,k)$. The RX can detect the presence of a target based on the strength of the 3D-DFT cube entry $\tilde{y}(i,j,k)$.

The beamformer $\mathbf{w}$ can potentially boost or attenuate $\alpha_p\mathbf{a}_{N_{\text{tx}}}(\theta_p)^T\mathbf{w}$, i.e., the effective RCS of the $p^{\text{th}}$ target. In the absence of any kind of side information on the scene, an omnidirectional beamformer that results in a uniform gain across all directions is a reasonable choice for $\mathbf{w}$. Such a beamformer, however, is suboptimal in typical automotive applications where side information is available. Beamformers that use side information can intelligently focus the available power to enhance radar detection in regions of interest, as will be discussed in the following section.

## 3. PROPOSED BEAMFORMING TECHNIQUE

To design the beamformer $\mathbf{w}$ at the TX, we assume that the 3D occupancy map $\mathbb{P}$, defined over the range-angle-Doppler bins, is known. Here, $\mathbb{P}(i,j,k)$ is the probability that there is a target in the $(i,j,k)^{\text{th}}$ bin.

Now, we discuss a binary hypothesis testing problem and analyze the probability of detecting a target in the $(i,j,k)^{\text{th}}$ bin as a function of $\mathbf{w}$. Let $(R_i, \Theta_j, \Omega_k)$ denote the range, angle and Doppler corresponding to the $(i,j,k)^{\text{th}}$ bin. We drop the target index $p$ in (3) to write down the received signal under two different hypotheses, i.e., the presence or the absence of a target. We define hypotheses $\mathcal{H}_0$ and $\mathcal{H}_1$ as

$$\mathcal{H}_0 : \tilde{y}(i,j,k) = \tilde{v}(i,j,k)$$
$$\mathcal{H}_1 : \tilde{y}(i,j,k) = \frac{\alpha_{i,j,k}\sqrt{P_{\text{tx}}}}{R_i^2}\mathbf{a}(\Theta_j)^T\mathbf{w} + \tilde{v}(i,j,k).$$

Although occupancy map information can be leveraged in the detection rule and beamformer design, we use a standard Neyman-Pearson detector in this paper and focus only on beamformer design. The probability that a target in the $(i,j,k)^{\text{th}}$ bin can be detected with this detector is [13]

$$P_{\text{d},\mathbf{w}}(i,j,k) = Q\left(Q^{-1}(P_{\text{FA}}) - \sqrt{\frac{P_{\text{tx}}}{R_i^4\sigma^2}|\alpha_{i,j,k}\mathbf{a}(\Theta_j)^T\mathbf{w}|^2}\right), \tag{4}$$

where $P_{\text{FA}}$ is the false alarm rate and $Q(\cdot)$ denotes the com-

plementary cumulative distribution function of the standard normal random variable. Due to the decreasing nature of the $Q(\cdot)$ function, we notice that $P_{\mathrm{d},\mathbf{w}}(i,j,k)$ is large at cells where a high beamforming gain is achieved.

Our beamforming technique aims to maximize the probability of detection at cells where there is a high uncertainty on the occupancy. Here, we use entropy as the measure of uncertainty, which can be expressed as a function of the occupancy probability. For the cell indexed $(i,j,k)$, the entropy associated with the occupancy probability of $\mathbb{P}(i,j,k)$ is

$$H(\mathbb{P}(i,j,k)) = -\mathbb{P}(i,j,k)\log_2(\mathbb{P}(i,j,k)) - (1-\mathbb{P}(i,j,k))\log_2(1-\mathbb{P}(i,j,k)). \quad (5)$$

We observe from (5) that the entropy achieves its maximum at cells where $\mathbb{P}(i,j,k) = 0.5$. We also notice that $H(\mathbb{P}(i,j,k)) = 0$ when $\mathbb{P}(i,j,k) = 0$ or $\mathbb{P}(i,j,k) = 1$. This is because there is no uncertainty associated with cells that are known to be free or those that are known to be occupied. Radars that scan cells with zero uncertainty do not provide any useful information.

A good sensing strategy is one that distributes the available power in a way that maximizes detection at cells associated with high uncertainty. To achieve this objective, we maximize a cost function that is a weighted sum of the probability of detections across all the cells. Here, the weights are set to the entropy values derived from the occupancy map. Our objective is a function of the beamformer $\mathbf{w}$, as the probability of detection in (4) depends on $\mathbf{w}$. The objective is maximized under the unit-norm constraint on $\mathbf{w}$ as shown in the formulation below.

$$\max_{\mathbf{w}} \sum_{i}^{N_{\mathrm{R}}} \sum_{j}^{N_{\mathrm{rx}}} \sum_{k}^{N_{\mathrm{D}}} H(\mathbb{P}(i,j,k)) P_{\mathrm{d},\mathbf{w}}(i,j,k) \quad \text{s.t.} \quad \|\mathbf{w}\|_2 \leq 1. \quad (6)$$

It can be shown that the maximization problem in (6) is non-concave. To solve the problem, we adopt the projected gradient ascent-based approach [14] to arrive at a locally optimal solution. In each iteration of this method, the TX computes the gradient of the cost function. Subsequently, it updates the beamformer in the direction of the gradient and projects the resultant vector onto the unit $\ell_2$ ball. These steps are repeated until the beamformer converges to a stationary point or when the number of iterations exceeds a predefined limit.

## 4. SIMULATION RESULTS

To evaluate the proposed approach, we solve the optimization problem in (6) and compare detection performance with the proposed beamformer against an omnidirectional beamformer. We use $N_{\mathrm{tx}} = 16$ antennas at the TX and $N_{\mathrm{rx}} = 16$ antennas at the RX, assuming perfect amplitude and phase control at all the elements of the TX array. We consider a bandwidth of $300\,\mathrm{MHz}$, which results in a range resolution of $0.5\,\mathrm{m}$. The maximum range of interest is set to $200\,\mathrm{m}$, which corresponds to $N_{\mathrm{R}} = 400$ range bins. The parameter $\alpha$ is set to $-68\,\mathrm{dB}$ for all the targets. Finally, the noise variance $\sigma^2$ is set to $-138\,\mathrm{dB}$ and the false alarm rate in (4) is $10^{-4}$.

In our evaluation, we use lane topology maps from the nuScenes dataset [15] to construct occupancy grid maps. The nuScenes topology maps contain labels for the plausible drivable space in different driving scenarios. We sample $500$ different driving scenarios and use the labels within each scene to construct an occupancy map $\mathbb{P}(i,j,k)$ that is faithful to the lane topology. Specifically, we set the occupancy probabilities of the cells in the drivable space to $0.5$ and the cells in the non-drivable space to $1$. This is because the cells in the non-drivable space are guaranteed to be occupied. Further, we assume that the number of Doppler bins is $N_{\mathrm{D}} = 1$ for computational tractability. The occupancy map is hence a 2D map in the range-angle domain. An example of the occupancy map derived from the nuScenes dataset is shown in Fig. 2a. Although we use maps that are just based on the lane topology, our beamformer design technique can also be applied for more realistic occupancy maps. Such maps can be estimated from a history of sensor point cloud data and vehicle motion models. The maps derived from the nuScenes dataset are used in (6) to design the beamformer for each scene.

We demonstrate the detection achieved by the proposed beamformer for scene 971 of the nuScenes dataset using Fig. 2. The scene in Fig. 2a shows that the drivable space extends up to about $80\,\mathrm{m}$ along the boresight direction and is limited to about $10\,\mathrm{m}$ towards the endfire. A good beamformer in this situation is one that focuses a higher power around the boresight than the endfire. We notice from Fig. 2a that such a beamformer is achieved with our design. We also observe from Fig. 2b that the proposed beamformer enhances target detection at cells with a higher entropy in the occupancy.

Next, we use scene 915 of the nuScenes dataset to explain the advantage of our approach over [12]. We notice from Fig. 3 that the drivable space spans two contiguous bands of directions. The method in [12] employs a beamformer that illuminates only the first band of directions, which is then steered to illuminate the second band. In contrast, our approach constructs a single beamformer such that the TX can illuminate both bands over the entire CPI. With the method in [12], the TX can look at each band for only half the CPI. Due to a higher effective CPI, the Doppler resolution with our approach is twice the resolution with [12] for this scene. Also, distributing the transmit power over the two bands reduces the beamforming gain. Therefore, a high Doppler resolution with our approach is achieved at the expense of a reduction in the probability of detection when compared to the use of a beamformer that covers just one band.

Finally, we assess the performance of the proposed approach for $500$ scenes chosen at random from the nuScenes dataset. Our metric, called weighted average probability of detection, is obtained by performing a weighted average of the probability of detection at the cells associated with a non-zero uncertainty. The weights are proportional to the entropy,

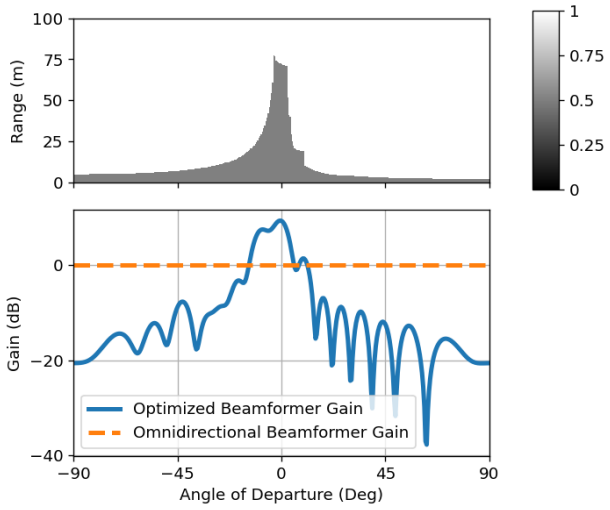


**(a)** Occupancy grid map (top) and the designed beamformer (bottom)

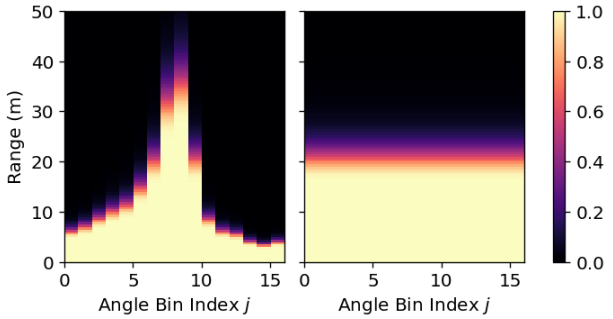


**(b)** Probability of detection achieved with the designed beam (left) and an omnidirectional beam (right)

**Fig. 2:** For $P_{\text{tx}} = 5\,\text{dB}$ and $N_{\text{rx}} = 16$, we show the occupancy grid map and the designed beamformer for scene 971 of the nuScenes dataset in (a). The probability of detection $P_{\text{d},\mathbf{w}}(i,j)$ achieved with our design and an omnidirectional beamformer are shown in (b). We observe that the proposed beamformer enhances detection in the region of interest defined by the occupancy map in (a).

and our metric is given by

$$\eta = \frac{\sum_{i,j,k} H(\mathbb{P}(i,j,k)) P_{d,\mathbf{w}}(i,j,k)}{\sum_{i,j,k} H(\mathbb{P}(i,j,k))}. \tag{7}$$

We observe from (7) that the detection probability at cells where the entropy is zero does not contribute to $\eta$. Fig. 4 shows a boxplot of $\eta$ obtained at different values of the transmitted power $P_{\text{tx}}$. Our designed beamformer consistently achieves a higher median weighted average probability of detection across different values of $P_{\text{tx}}$. At lower levels of $P_{\text{tx}}$, the performance of our beamformer approaches that of an omnidirectional beamformer, as the available power is spread more widely across the drivable space near the vehicle. We also observed that our method achieves similar performance as the standard beamformer when $P_{\text{tx}} > 25\,\text{dB}$. This is because an omnidirectional beamformer is sufficient to achieve good detection at high power levels.

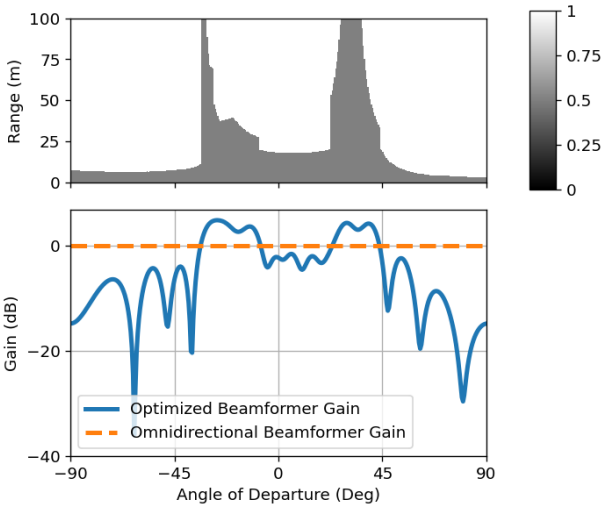


**Fig. 3:** We show the occupancy grid map and the designed beamformer for scene 915 of the nuScenes dataset. Here, the transmit power $P_{\text{tx}} = 5\,\text{dB}$. We observe that our method can generate multi-armed beam patterns that are well-suited to the occupancy map.

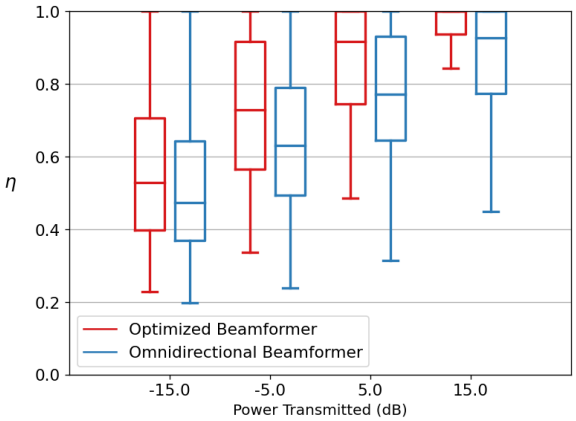


**Fig. 4:** Boxplot of the weighted average detection probabilities obtained for 500 scenes in the nuScenes dataset. The designed beamformers achieve a higher detection probability in the regions of interest than the omnidirectional beamformer.

## 5. CONCLUSION AND FUTURE WORK

We developed a transmit beamforming method for automotive radar applications to incorporate prior information on the scene being sensed. The prior information, in the form of an occupancy map, was used to determine the entropy at different cells in the scene. By using entropy-based weighting over the detection probabilities, our method optimizes the transmit beamformer to achieve a higher probability of detection in regions with high uncertainty than the omnidirectional beamformer. Simulation results over the nuScenes dataset indicate that our adaptive beamforming technique performs well for different lane topologies. In the future, we will extend our technique by relaxing assumptions such as known noise variance and a clutter-free environment.

## 6. REFERENCES


[1] C. Waldschmidt, J. Hasch, and W. Menzel, "Automotive radar — from first efforts to future systems," *IEEE J. Microw.*, vol. 1, no. 1, pp. 135–148, 2021.

[2] F. Engels, P. Heidenreich, M. Wintermantel, L. Stäcker, M. Al Kadi, and A. M. Zoubir, "Automotive Radar Signal Processing: Research Directions and Practical Challenges," *IEEE J. Sel. Top. Signal Process.*, vol. 15, no. 4, pp. 865–878, 2021.

[3] S. Sun, A. P. Petropulu, and H. V. Poor, "MIMO Radar for Advanced Driver-Assistance Systems and Autonomous Driving: Advantages and Challenges," *IEEE Signal Process. Mag.*, vol. 37, no. 4, pp. 98–117, 2020.

[4] M. Bijelic, T. Gruber, F. Mannan, F. Kraus, W. Ritter, K. Dietmayer, and F. Heide, "Seeing through fog without seeing fog: Deep multimodal sensor fusion in unseen adverse weather," in *Proc. IEEE/CVF Conf. Comput. Vis. Pattern Recognit. (CVPR)*, 2020, pp. 11 682–11 692.

[5] R. Prophet, A. Deligiannis, J.-C. Fuentes-Michel, I. Weber, and M. Vossiek, "Semantic Segmentation on 3D Occupancy Grids for Automotive Radar," *IEEE Access*, vol. 8, pp. 197 917–197 930, 2020.

[6] F. Gies, A. Danzer, and K. Dietmayer, "Environment perception framework fusing multi-object tracking, dynamic occupancy grid maps and digital maps," in *Proc. Int. Conf. Intell. Transp. Syst. (ITSC)*, 2018, pp. 3859–3865.

[7] M. Schreier, V. Willert, and J. Adamy, "Compact representation of dynamic driving environments for adas by parametric free space and dynamic object maps," *IEEE Trans. Intell. Transp. Syst.*, vol. 17, no. 2, pp. 367–384, 2016.

[8] J. S. Bergin, C. M. Teixeira, P. M. Techau, and J. R. Guerci, "Improved clutter mitigation performance using knowledge-aided space-time adaptive processing," *IEEE Trans. Aerosp. Electron. Syst.*, vol. 42, no. 3, pp. 997–1009, 2006.

[9] C.-Y. Chen and P. Vaidyanathan, "MIMO radar waveform optimization with prior information of the extended target and clutter," *IEEE Trans. Signal Process.*, vol. 57, no. 9, pp. 3533–3544, 2009.

[10] P. Wirfält, M. Jansson, G. Bouleux, and P. Stoica, "Prior knowledge-based direction of arrival estimation," in *Proc. IEEE Int. Conf. Acoust. Speech Signal Process. (ICASSP)*, 2011, pp. 2540–2543.

[11] G. Bouleux, P. Stoica, and R. Boyer, "An optimal prior-knowledge-based DOA estimation method," in *Proc. Eur. Signal Process. Conf. (EUSIPCO)*, 2009, pp. 869–873.

[12] Z. W. Johnson and R. A. Romero, "Adaptive beamsteering cognitive radar with integrated search-and-track of swarm targets," *IEEE Access*, vol. 9, pp. 50 652–50 666, 2021.

[13] M. A. Richards, *Fundamentals of Radar Signal Processing*. McGraw-Hill Professional, 2005.

[14] S. P. Boyd and L. Vandenberghe, *Convex optimization*. Cambridge university press, 2004.

[15] H. Caesar, V. Bankiti, A. H. Lang, S. Vora, V. E. Liong, Q. Xu, A. Krishnan, Y. Pan, G. Baldan, and O. Beijbom, "nuScenes: A multimodal dataset for autonomous driving," in *Proc. IEEE/CVF Conf. Comput. Vis. Pattern Recognit. (CVPR)*, 2020, pp. 11 621–11 631.